

1 **Brief communication: Two well marked cases of aerodynamic
2 adjustment of sastrugi**

3 **C. Amory^{1,2,3,4}, F. Naaim-Bouvet^{3,4}, H. Gallée^{1,2} and E. Vignon^{1,2}**

4 [1]{Univ. Grenoble Alpes, LGGE, F-38041 Grenoble, France}

5 [2]{CNRS, LGGE, UMR5183, 38401 Grenoble, France}

6 [3]{Univ. Grenoble Alpes, IRSTEA, F-38041 Grenoble, France}

7 [4]{IRSTEA, UR ETNA, F-38402 Saint-Martin d'Hères, France}

8

9 Correspondence to: C. Amory (amory@lgge.obs.ujf-grenoble.fr)

10

11 **Keywords:** Antarctica - Drag coefficient - Drifting snow - Sastrugi aerodynamic adjustment -
12 Sastrugi form drag

13 **Abstract**

14 In polar regions, sastrugi are a direct manifestation of drifting snow and form the main surface
15 roughness elements. In turn, sastrugi alter the generation of atmospheric turbulence and thus
16 modify wind profiles and aeolian snow mass fluxes. Little attention has been paid to these
17 feedback processes, mainly because of experimental difficulties, and, as a result most polar
18 atmospheric models currently ignore sastrugi. This paper focuses on two cases during which
19 sastrugi responses to shifts in wind direction were evidenced by variations in aeolian snow mass
20 fluxes and neutral stability 10-m air-snow drag coefficients C_{DN10} computed from wind profiles
21 collected during austral winter 2013 in coastal Adélie Land, East Antarctica. Using this dataset,
22 it was shown that (i) C_{DN10} values were in the range of $1.3-1.5 \times 10^{-3}$ when the wind was well
23 aligned with the sastrugi and could increase to nearly 3.3×10^{-3} with wind shifts of only 20-
24 30°, (ii) as C_{DN10} increases, the aeolian snow mass flux can decrease (to 80%) in response to a
25 shift in wind direction, (iii) the timescale of sastrugi aerodynamic adjustment can be as short as
26 3 h for friction velocities of 1 m s^{-1} or above and during strong drifting snow conditions, and
27 (iv) knowing C_{DN10} is not sufficient to estimate the erosion flux that results from drag
28 partitioning at the surface because C_{DN10} includes the contribution of the sastrugi form drag.

29 **1. Introduction**

30 In polar regions, sastrugi are a direct manifestation of drifting snow. They are generally
31 regarded as elongated ridges of wind-packed snow 1 to 2 meters in length whose longitudinal

1 axis is parallel to the prevailing wind at the time of their formation. These erosional surface
2 roughness features are very widespread over the Antarctic ice sheet (Kotlyakov 1961) where
3 they can be major determinants of surface roughness (Jackson and Carroll 1978; Inoue 1989;
4 Andreas and Claffey 1995). Sastrugi orientations have been recognized as useful indicators of
5 the Antarctic near-surface wind direction (Mather 1962, 1969; Mather and Miller 1966; Long
6 and Drinkwater 2000) in agreement with continent-scale modeling studies (Parish and
7 Bromwich 1987, 2007).

8 The development of sastrugi depends on the ability of snow to be eroded and thus on the
9 threshold velocity needed to lift snow particles from the surface. In the literature, aeolian
10 erosion thresholds have been reported to vary depending on temperature and diverse properties
11 of surface snow. From observations in Antarctica, Mellor (1965) reported that 10-m wind
12 speeds of 3 to 8 m s^{-1} are strong enough to cause aerodynamic entrainment of loose, unbounded
13 snow, whereas winds exceeding 30 m s^{-1} are needed to erode snow consolidated by the freeze-
14 thaw process. Budd et al. (1966) suggested a high threshold wind speed (14 m s^{-1}) was needed
15 to trigger snow transport in the cold environment of Byrd station. Schmidt (1980) reported that
16 the cohesion of the snow surface determines the threshold speed required for snow erosion to
17 occur. Schmidt (1980) also showed that the threshold wind speed increases with time since
18 snow deposition, and that this increase slows with time and is slower at lower temperatures.
19 Pomeroy et al. (1993) identified significantly lower thresholds for fresh, loose, dry snow than
20 for older, wind hardened, dense or wet snow. Oura et al. (1967) and, later on, Li and Pomeroy
21 (1997) discussed the major role of temperature in surface erodibility (i.e. the potential of a
22 surface to be eroded; Shao 2008) through metamorphism of snow (i.e. changes in snow
23 structure over time), and showed an empirical but generally positive correlation between
24 threshold wind speed and air temperature. All studies suggest that the physical properties of the
25 snow play a major role in the formation of sastrugi.

26 Sastrugi contribute to the drag exerted on the atmosphere over the snow surface and enhance
27 interactions at the air-snow interface compared to over a smooth snow surface. Rougher snow
28 surfaces favor the generation of turbulence in the near surface air stream that is likely to further
29 increase the aeolian snow mass flux (Das et al. 2013). On the other hand, sastrugi are
30 responsible for a loss of wind momentum through pressure fluctuation gradients in their
31 immediate vicinity (sastrugi form drag) that directly reduces the energy budget available for
32 erosion of snow. This attenuating effect on snow erosion is taken into account in the coupled
33 atmosphere-snowpack-aeolian snow transport model MAR (Gallée et al. 2013) and was
34 parametrized as in Marticorena and Bergametti (1995). By comparing observed and simulated

1 aeolian snow mass fluxes over Adélie Land using MAR, Amory et al. (2015) showed that in
2 the model, erosion efficiency is highly sensitive to the parameterization of surface roughness,
3 and underlined the need for observational characterization of interactions between wind-
4 induced roughness features and aeolian transport of snow.

5 Some authors have shown that the sastrugi form drag actually depends on how the wind is
6 oriented with respect to the main sastrugi axis. Based on measurements of wind speed and
7 temperature profile in the atmospheric surface layer at the South Pole, Jackson and Carroll
8 (1978) reported that sastrugi form drag was essentially absent when the wind was perfectly
9 aligned with the sastrugi up to a height of 50 cm. As the wind rotated, sastrugi form drag
10 increased, to reach maximum when the wind direction was perpendicular to the prior sastrugi
11 pattern. These authors developed an idealized single sastruga model from Lettau's (1969)
12 findings to reproduce their observations. Using another analytical sastruga model adapted from
13 Raupach (1992), Andreas (1995) also found a minimum and a maximum drag for wind
14 directions respectively parallel and perpendicular to the sastruga longitudinal axis. However,
15 these modeling efforts were undertaken without accounting for the erodible character of
16 sastrugi or for their possible reorganization when realigning with persistent (erosive) winds
17 blowing transversally to their elongated sidewalls. If the crosswise flow continues from a
18 relatively constant direction thereby allowing sufficient shear stress to dislodge snow surface
19 particles, sastrugi can adjust aerodynamically; transversal sastrugi are eroded, and new
20 streamlined sastrugi form parallel to the mean wind (Andreas and Claffey 1995). This results
21 in a gradual decrease in the contribution of the sastrugi to the total surface drag, and hence in
22 an increase in erosion efficiency. Andreas and Claffey (1995) reported that the timescale for
23 this streamlining process on Weddell Sea ice in winter was about half a day with $6-8 \text{ m s}^{-1}$
24 winds, but might be shorter if the winds are stronger. To date, no observational study has
25 provided quantitative insight into the potential effect of erodible roughness elements of the
26 snow surface on snow erosion.

27 Quantifying the variable influence of sastrugi on the local wind field and associated surface
28 drag could improve parameterization of surface roughness and erosion in polar atmospheric
29 models that currently ignore sastrugi. The present paper focuses on two erosion events during
30 which sastrugi responses to shifts in wind direction were interpreted from temporal variations
31 in both measured drag and aeolian snow mass flux in coastal Adélie Land during austral winter
32 2013.

33 **2. Data and Method**

1 **2.1. Field area**

2 Site D17 (66.7°S, 139.9°E; ~450 m asl.) is located about 10 km inland in a coastal accumulation
3 zone of Adélie Land (Agosta et al. 2012), roughly 15 km southwest of the permanent French
4 station Dumont d'Urville (Fig. 1). An annual temperature of -10.8 °C and a mean wind of
5 around 10 m s⁻¹ have been reported at Dumont d'Urville station (König-Langlo et al. 1998).
6 The measurement area consists in a gently sloping snowfield with a long unobstructed upstream
7 fetch several hundred kilometers over a uniform snow surface. Local topographic channeling
8 acts together with the Coriolis force to produce southeasterly flows all year round that result
9 either from pure katabatic or combined katabatic-synoptic forcings (Parish et al. 1993).
10 Site D17 is visited only during summer (December to February), when the presence of sastrugi
11 is often reported. Frequent strong winds combined with the permanent snow surface lead to
12 frequent aeolian snow transport events (Trouvilliez et al. 2014), thereby favoring aerodynamic
13 adjustment of the snow surface. This results in a net south-southeast orientation of the sastrugi
14 (Fig. 2).

15 **2.2. Instrumentation**

16 The measurement structure deployed at site D17 is a 7-m high meteorological mast. Wind
17 speed, relative humidity and air temperature are recorded along the mast at 6 logarithmically
18 spaced intervals between 0.8 and 7 m above the snow surface using Vector A100LK cup
19 anemometers and HMP45A thermo-hygrometers installed in naturally ventilated MET21
20 radiation shields. The anemometers are mounted on roughly 1-m long booms pointing
21 southeastward. Wind direction is only sampled at the upper level by a Vector W200P wind
22 vane. Surface level variations are measured by a Campbell SR50A acoustic depth gauge.
23 Information on drifting snow is obtained from a second-generation acoustic FlowCapt™ device
24 that was set up vertically close to the ground to allow detection of the beginning of aeolian
25 snow transport events. The sensor is a 1-m long tube that converts the acoustic pressure caused
26 by snow particles impacting the tube into an aeolian snow mass flux integrated over the length
27 of the tube. The second-generation FlowCapt™ was evaluated in the French Alps by Trouvilliez
28 et al. (2015). The authors reported that the instrument underestimates the aeolian snow mass
29 flux compared to a reference optical sensor (Snow Particle Counter S7; Sato et al. 1993),
30 especially during snowfalls. Nevertheless, the equivocal behavior of the second-generation
31 FlowCapt™ does not affect its ability to accurately detect the occurrence of aeolian snow

1 transport. Data were sampled at 15 s intervals, averaged to half-hourly means and stored in a
2 Campbell CR3000 datalogger.

3 **2.3. The 10-m drag coefficient in near-neutral conditions**

4 Computing the drag coefficient (C_D) is a convenient way to estimate the local drag exerted by
5 the surface on the overlying air. C_D can be computed by measuring the vertical wind speed
6 gradient (profile method) under near-neutral conditions following the Monin-Obukhov
7 similarity theory. Assuming stationarity and horizontal homogeneity when the atmospheric
8 surface layer is statically neutral, the wind speed profile is logarithmic and can be written as

$$U(z) = \frac{u_*}{\kappa} \ln \left(\frac{z}{z_0} \right), \quad (1)$$

9 where $U(z)$ is the average wind speed as a function of height z , κ is the von Kármán constant
10 (taken as 0.4), z_0 is the aerodynamic roughness length, and u_* the friction velocity describing
11 the wind shear at the surface and being related to the vertical momentum flux at the surface (τ ;
12 also known as Reynolds shear stress)

$$\tau = \rho u_*^2 = -\rho \bar{u} \bar{w} = \rho C_{DNz} U_z^2, \quad (2)$$

13 where ρ is the air density, u and w are fluctuations in the longitudinal and vertical turbulent
14 velocity, respectively, and C_{DNz} and U_z are the neutral-stability drag coefficient and the average
15 wind speed at height z , respectively. The overbar stands for a time average. C_{DN} is usually
16 discussed at a standard reference height of 10 m (C_{DN10}). From (2) and (3), it follows that

$$C_{DN10} = \left[\kappa / \ln \left(\frac{10}{z_0} \right) \right]^2, \quad (3)$$

17 with z_0 expressed in meters. Here C_{DN10} and z_0 are two equivalent quantities for evaluating the
18 momentum exchange at the air-snow interface that results from the integrated (in space and
19 time) turbulent drag caused by the roughness elements.

20 The wind profiles used to compute C_{DN10} were selected following a strict procedure. After
21 discarding icing or malfunctioning cases and half-hourly runs for which a rare (northwesterly)
22 flow was likely to be disturbed by the measurement structure, stationary conditions were
23 selected by requiring that temperature changes between two consecutive half-hourly runs not
24 exceed 0.3 K, following Joffre (1982)'s recommendations. Near-neutral conditions were then
25 selected requiring $U > 5 \text{ m s}^{-1}$ and an absolute value of the bulk Richardson number below 10⁻

1 ². The last selection criterion was applied following a suggestion by Andreas and Claffey (1995)
2 that demands

3

$$\frac{\sum_{i=1}^6 [U(z_i) - (u_*/\kappa) \ln(z_i/z_0)]^2}{u_*^2} \leq \varepsilon, \quad (4)$$

4
5 where ε is an empirical constant determined from visual inspection of the observed wind speed
6 profiles. Here it was set to 0.15. Wind profiles that survived this filtering process were fitted
7 (1) using a least-square log-linear regression technique, and u_* and z_0 deduced from the
8 regression coefficients. All of them yielded a correlation coefficient (r^2) larger than 0.99. The
9 80% confidence limits of each calculated C_{DN10} value were determined following the statistical
10 method proposed by Wilkinson (1984). The highest uncertainty bounds deduced from these
11 confidence limits reached $\pm 14\%$.

12 **3. Results**

13 The two erosion events depicted in Figure 3 occurred respectively in March (left panels) and
14 October (right panels), 2013, during particularly constant wind direction conditions, which
15 persisted after a wind shift of a few tens of degrees. Such a constancy in wind direction,
16 necessary for the following demonstration, is very rare. Combined to the strict selection
17 procedure, only two cases were exploitable in this context. The 2-m wind speed, wind direction,
18 profiled-derived C_{DN10} values and aeolian snow mass flux recovered by the second-generation
19 FlowCapt™ sensor are shown in Figure 3. As the friction velocity is the actual dynamic quantity
20 involved in aerodynamic entrainment of surface snow particles, it is also plotted on the graph.
21 The two events are split into three parts, before (A_i), during (B_i) and after (C_i) the shift in wind
22 direction. The occurrence of precipitation may affect the detection of erosion events because
23 the FlowCapt™ sensor does not distinguish between eroded (saltating particles and/or
24 suspended particles of snow) and precipitating snow particles. No visual observation of
25 precipitation from the nearby Dumont d'Urville station were available for the period concerned.
26 Moreover, as Adélie Land is very prone to aeolian transport of snow, these observations, if
27 performed, are limited by the inability to discriminate between actual precipitation and pure
28 drifting snow. Here we used the operational analyses of the European Center for Medium-
29 Range Weather Forecasts (horizontal resolution of ~ 16 km) to evaluate the occurrence of
30 precipitation at our measurement site. We assumed that both events were pure erosion events

1 after finding negligible precipitation rates for the fully continental grid point including D17.
2 At the beginning of Julian day (JD) 87 (part A₁), the wind direction was around 140°, the
3 friction velocity was above the erosion threshold with a related aeolian snow mass flux of 100
4 g m⁻² s⁻¹, and C_{DN10} was near 1.5×10^{-3} . At the end of JD 87 (part B₁), the wind rotated toward
5 160° while C_{DN10} increased to nearly 3.3×10^{-3} , i.e. by 120%, in response to a wind shift of
6 only 20°. As assumed in Jackson and Carroll (1978) and Andreas and Claffey (1995), it is likely
7 that as the wind turned, it was deflected from the mean sastrugi axis, thereby encountering a
8 rougher surface. As a result, C_{DN10} soared, reflecting the growing contribution of the sastrugi
9 form drag to the vertical momentum flux at the surface, and hence to the total surface drag.
10 Within the same time frame, the measured aeolian snow mass flux fell by ~30% from 365 to
11 260 g m⁻² s⁻¹, despite increasing friction velocity (wind speed) from 0.7 to 1.6 (18 to 24) m s⁻¹.
12 Then, until the end of the event (part C₁), the wind direction remained centered about 160°.
13 From 0330 UT to 0630 UT on JD 88, C_{DN10} fell back to 1.5×10^{-3} as high winds presumably
14 streamlined the surface. In other words, C_{DN10} was reduced by ~50% in only 3 hours. As C_{DN10}
15 decreased, the aeolian snow mass flux again rose above 400 g m⁻² s⁻¹. The erosion event lasted
16 through JD 90 when u_* (wind speed) dropped to 0.7 (15) m s⁻¹, causing a significant decrease
17 in the aeolian snow mass flux. After nearly 48 hours of persistent erosive winds, C_{DN10} was as
18 low as 1.3×10^{-2} .
19 During the two days that preceded the second erosion event (part A₂), the wind direction was
20 within $\pm 10^\circ$ of 150°, the friction velocity was generally not strong enough to erode the snow
21 surface, and C_{DN10} was between $1.3 - 1.6 \times 10^{-3}$. C_{DN10} and wind direction were strongly
22 correlated during this period, with the lowest drag coefficients occurring for a wind direction
23 of around 140°, suggesting that this was the sastrugi alignment before erosion started and the
24 wind changed direction. Then, the same situation depicted in the left panels of Figure 3 occurred
25 again. At mid-JD 286 (part B₂), u_* increased beyond the erosion threshold as the wind rotated
26 from 150° to 180°. Consequently, C_{DN10} increased to 1.9×10^{-3} . The aeolian snow mass flux
27 dropped simultaneously from 320 to 55 g m⁻² s⁻¹ under increasing friction velocity. That is, for
28 a ~30% increase in C_{DN10} as the result of a wind deflection of 30°, the aeolian snow mass flux
29 decreased by ~80%. Together with the first case of erosion, this illustrates how the form drag
30 exerted by sastrugi can significantly affect snow erosion when the wind and sastrugi are not
31 aligned (this effect is discussed later in the paper; see Section 4). Then (part C₂), the wind
32 direction remained roughly unchanged until erosion ceased. Again, the rise in aeolian snow

1 mass flux coincided with a decrease in C_{DN10} . After nearly 3 hours of winds above 20 m s^{-1} ($u_* > 0.9 \text{ m s}^{-1}$) from 180° , C_{DN10} fell from 1.9×10^{-3} to 1.4×10^{-3} , i.e. decreased by $\sim 30\%$.
2 In summary, for friction velocities (wind speeds) around 1 (20) m s^{-1} and above, the sastrugi
3 streamlining timescale can be as fast as 3 hours. For a windflow initially aligned with the
4 sastrugi, a deviation of 20 - 30° from the streamlining direction has the potential to both increase
5 C_{DN10} by 30 - 120% and to significantly reduce (up to 80%) the aeolian snow mass flux, even
6 under increasing friction velocity.
7

8 4. Discussion

9 At Ice Station Weddell, Andreas and Claffey (1995) measured a decrease in C_{DN10} of 20 - 30%
10 in 12 hours with considerably weaker winds ($< 12 \text{ m s}^{-1}$) than those reported here. The
11 observations reported in this paper show that this timescale can be 4 times faster for winds
12 exceeding 20 m s^{-1} ($u_* > 1 \text{ m s}^{-1}$), and the associated decrease in C_{DN10} can reach 50% . Andreas
13 and Claffey (1995) also proposed generic C_{DN10} values in the range 1.5 - 1.7×10^{-3} when the
14 wind is well aligned with the sastrugi, and around 2.5×10^{-3} when the wind is at an angle of 20°
15 to the dominant orientation of the sastrugi. The present results differ slightly from these values:
16 C_{DN10} was more in the range 1.3 - 1.5×10^{-3} for sastrugi-parallel winds, and could increase to
17 more nearly 3.4×10^{-3} with a wind shift of similar amplitude. For a given erosion threshold, the
18 quantity of windborne snow increased with wind strength according to a power law (Mann
19 2000). As sastrugi mainly form through snow erosion/deposition processes (Filhol and Sturm
20 2015), it is likely that under the strong wind (shear) conditions in Adélie Land, rougher snow
21 surfaces develop, whose aerodynamic adjustment ability is greater than at the less windy Ice
22 Station Weddell.

23 During both erosion events, significant aeolian snow mass fluxes were measured for 2-m wind
24 speeds (u_*) of 10 (0.6) m s^{-1} or above. As the wind (friction) velocity likely frequently exceeds
25 this threshold on the coastal slopes of Adélie Land, the sastrugi alignment process might be
26 also frequently active, depending on persistence of the wind. As explained in Section 1, this
27 mechanism is probably also strongly controlled by the properties of the snow surface that
28 determine the threshold shear stress required for erosion to begin rather than only the
29 characteristics of the wind. Since the erosion flux is the integrated result of both the capacity of
30 the wind to erode and carry snow, and snow surface erodibility, the sastrugi streamlining
31 timescale presumably mostly depends on this specific quantity. The implication is that the drag
32 coefficient must be strongly related to other factors including the current wind orientation and

1 the history of the wind's interactions with the snow surface as well as past timescales and past
2 temperatures of the snowpack.

3 On the other hand, the sastrugi streamlining timescale also appears to control snow erosion in
4 the form of feedback by fixing the time during which the sastrugi form drag mainly contributes
5 to total surface drag. With friction velocities above the snow erosion threshold, increasing u_*
6 could be expected to result in an increase in erosion efficiency. However, in both cases, the
7 observations showed a significant decrease in the aeolian snow mass flux in phase with an
8 increase in the drag coefficient (Figure 3, parts B). By analogy with measurements made in a
9 water flume (Wiberg and Nelson 1992; Le Bouteiller and Venditti 2015), it can be considered
10 that the flow and turbulence in the sastrugi region are the result of interaction between flow
11 separation and wake formation, which can lead to a local Reynolds shear stress peak
12 corresponding to flow separation. Above the region of influence of the wake, named outer
13 region, the flow has adjusted to increased roughness and exhibited a logarithmic profile, as
14 shown by the relative continuous time series of C_{DN10} and u_* (Fig. 3) despite the strict selection
15 procedure. Even if the shear stress of the outer flow (τ) is relatively easy to measure, it cannot
16 be extrapolated to the snow bed. The averaged snow bed shear stress (also referred to as skin
17 friction in the literature), which is the ultimate parameter for aeolian erosion (Li and Shao
18 2003), varies depending on its position along the sastrugi field. In absence of direct
19 measurements, it is necessary to link outer shear stress, sastrugi geometry, and skin friction to
20 be able to estimate aeolian snow mass fluxes. This is quite important since the reduction of
21 shear stress near the surface is crucial in limiting the growth of the mass flux (Groot Zwaftink
22 et al., 2014). For erodible forms in riverbeds such as ripples, Smith and McLean (1977) and
23 later Wiberg and Nelson (1992) developed a method for partitioning the outer shear stress.
24 These authors considered that the averaged bed shear stress is equal to the difference between
25 the outer shear stress and the drag-related stress produced as the flow is forced around the
26 bedform – i.e., in the present case, the form drag induced by the sastrugi. As mentioned above,
27 an increasing form drag can be expected, and hence a decrease in skin friction and in aeolian
28 snow mass flux, when the wind direction gradually shifts away from the longitudinal axis of
29 the sastrugi. Because C_{DN10} reflects the contribution of the sastrugi form drag, knowing the
30 drag coefficient is not sufficient to estimate skin friction. A better knowledge of skin friction
31 over a sastrugi field is also needed to improve aeolian snow mass flux parameterizations in
32 aeolian erosion models. The measurements made in the present study showed that a
33 considerable decrease (even 80%) of the aeolian snow mass flux can occur during the
34 transitional regime during which the wind and sastrugi are not aligned (Figure 3, parts B). But

1 it should be also noted that the rapid aerodynamic adjustment of sastrugi (3 hours) will limit
2 errors if the erosion event considered is strong and sufficiently long.

3 **5. Conclusion**

4 An experimental meteorological dataset collected in coastal Adélie Land during austral winter
5 2013 was exploited to document surface turbulent fluxes of momentum and snow over an
6 Antarctic sastrugi field. The main results of the analysis of two erosion events can be
7 summarized as follows:

8 - C_{DN10} values were in the range of $1.3-1.5 \times 10^{-3}$ when the wind was well aligned with
9 sastrugi and could increase to nearly 3.3×10^{-3} with wind shifts of only $20-30^\circ$,
10 - As C_{DN10} increases, the aeolian snow mass flux may decrease (to 80%) in response to
11 the wind shift in direction,
12 - the timescale for the aerodynamic adjustment of sastrugi can be as low as three hours
13 for friction velocities of 1 m s^{-1} or above and during strong drifting snow conditions,
14 - because C_{DN10} includes the contribution of the sastrugi form drag, knowing C_{DN10} is
15 not sufficient to estimate the erosion flux that results from drag partitioning at the
16 surface.

17 These results support the existence of feedback mechanisms linking aeolian erosion and surface
18 drag properties over (Antarctic) snow surfaces, as already demonstrated for other erodible
19 natural surfaces (Marticorena and Bergametti 1995). In contrast with non-erodible roughness
20 elements such as rocks or vegetation, these mechanisms involve the time needed for sastrugi to
21 adjust to the main wind (3 hours in both erosion events), during which both the drag coefficient
22 and the aeolian snow mass flux can be greatly modified. In comparison, Andreas and Claffey
23 (1995) reported a longer timescale (12 hours) for the sastrugi to realign with weaker winds.
24 Because lighter winds are supposed to be associated with lower erosion fluxes, it is suggested
25 that the sastrugi streamlining timescale most likely depends on the snow erosion flux.

26 Real-time observations of the distribution (size, abundance, orientation) of the sastrugi would
27 further advance understanding of the physical processes involved in the development of sastrugi
28 and enable better characterization of sastrugi aerodynamic adjustment timescales. In addition,
29 having a more accurate representation of the distribution of sastrugi would make small-scale
30 modeling in a wind tunnel possible, in which case, it would be possible to realistically estimate
31 shear stress partitioning. One possible way to monitor sastrugi would be to set up an automatic

1 mini laser-scan. Such a device was developed in the framework of the MONISNOW research
2 project (Picard and Arnaud, LGGE, personal communication) and has been operating daily at
3 Dome C in Antarctica since the beginning of 2015. These complementary approaches are vital
4 to improve parameterization schemes for aeolian snow transport models and general drag
5 parameterizations for weather, climate and earth system models.

6 **References**

7 Amory, C., Trouvilliez, A., Gallée, H., Favier, V., Naaim-Bouvet, F., Genthon, C., Agosta,
8 C., Piard, L., and Bellot, H., 2015. Comparison between observed and simulated aeolian snow
9 mass fluxes in Adélie Land, East Antarctica. *The Cryosphere*, 9, 1–12.

10 Andreas, E. L., 1995. Air-ice drag coefficients in the western weddell sea. 2. A model based on
11 form drag and drifting snow. *J. Geophys. Res.*, 100(C3), 4833–4843.

12 Andreas, E. L. and Claffey, K. J., 1995. Air-ice drag coefficients in the western weddell sea. 1.
13 Values deduced from profile measurements. *J. Geophys. Res.*, 100(C3), 4821–4831.

14 Budd, W. F., 1966. The drifting of non-uniform snow particles. *Studies in Antarctic
15 Meteorology*, M. J. Rubin, Ed., Antarctic Research Series, Vol. 9, American Geophysical
16 Union, 59-70.

17 Das, I., Bell, R. E., Scambos, T. A., Wolovick, M., Creyts, T. T., Studinger, M., Frearson, N.,
18 Nicolas, J. P., Lenaerts, J. T. M., and van den Broeke, M. R., 2013. Influence of persistent wind
19 scour on the surface mass balance of Antarctica, *Nat. Geosci.*, 6, 367–371.

20 Filhol, S., and Sturm, M., 2015. Snow bedforms: A review, new data and a formation model.
21 *J. Geophys. Res.*, 120, 9, 1645-1669. doi: 10.1002/2015JF003529.

22 Gallée, H., Trouvilliez, A., Agosta, C., Genthon, C., Favier, V., and Naaim-Bouvet, F., 2013.
23 Transport of Snow by the Wind: A Comparison Between Observations in Adélie Land,
24 Antarctica, and Simulations Made with the Regional Climate Model MAR. *Boundary-Layer
25 Meteorol.*, 146, 133–147.

26 Groot Zwaftink, C. D., Diebold, M., Horender, S., Overney, J., Lieberherr, G., Parlange, M.,
27 and Lehning, M., 2014. Modelling small-scale drifting snow with a Lagrangian stochastic
28 model based on large-eddy simulations. *Boundary-Layer Meteorol.*, 153, 117–139,

1 doi:10.1007/s10546-014-9934-2.

2 Inoue, J., 1989. Surface drag over the snow surface of the Antarctic Plateau. 1: factors
3 controlling surface drag over the katabatic wind region. *J. Geophys. Res.*, 94, 2207-2217.

4 Joffre, S. M., 1982. Momentum and heat transfers in the surface layer over a frozen sea.
5 *Boundary-Layer Meteorol.*, 24, 211-229.

6 König-Langlo, G., King, J. C., and Pettré, P., 1998. Climatology of the three coastal Antarctic
7 stations Dumont d'Urville, Neumayer, and Halley. *J. Geophys. Res.*, 103(D9), 10,935-10,946,
8 doi:10.1029/97JD00527.

9 Kotlyakov, V. M., 1961. The Snow Cover of the Antarctic and its role in the Present-Day
10 Glaciation of the Continent (Snezhni pokrov antarktidy i ego rol' v somvremennom oledenenii
11 materika), Translated from Russian 1966, Israel Program for Scientific Translation, Jerusalem,
12 256 p.

13 Lettau, H. H., 1969. Note on aerodynamic roughness-parameter estimation on the basis of
14 roughness element description. *Journal of Applied Meteorology*, 8, 828-832.

15 Li, L., and Pomeroy, J. W., 1997. Estimates of Threshold Wind Speeds for Snow Transport
16 Using Meteorological Data. *J. Appl. Meteorol.*, 36, 205-213.

17 Li, A., and Shao, Y., 2003. Numerical simulation of drag partition over rough surfaces.
18 *Boundary-Layer Meteorol.*, 108, 317-342.

19 Le Bouteiller, C., and Venditti, J. G., 2015. Sediment transport and shear stress partitioning in
20 a vegetated flow. *Water Resour. Res.*, 51, 2901-2922, doi:10.1002/2014WR015825.

21 Long, D. G., and Drinkwater, M. R., 2000. Azimuth variation in microwave scatterometer and
22 radiometer data over Antarctica. *Transactions on Geoscience and Remote Sensing*, 38,
23 1857-1870.

24 Marticorena, B., and Bergametti, G., 1995. Modeling the atmospheric dust cycle: 1. Design of
25 a soil-derived dust emission scheme. *J. Geophys. Res.*, 100, 16415-16430.

26 Mather, K. B., 1962. Further observations on sastrugi, snow dunes and the pattern of surface
27 winds in Antarctica. *The Polar Record*, 11, 158-171.

1 Mather, K. B., 1969. The pattern of surface wind flow in Antarctica. *Pure and Applied*
2 *Geophysics*, 75, 332-354.

3 Mather, K. B., and Miller, G. S., 1966. Wind drainage off the high plateau of Eastern Antarctica.
4 *Nature*, 209, 281-284.

5 Mellor, M., 1965. Blowing snow. *CRREL MonographIII*, A3c, Cold Regions Res. And Eng.
6 Lab., Hanover, N.H.

7 Naaim-Bouvet, F., Bellot, H., and Naaim, M., 2010. Back analysis of drifting-snow
8 measurements over an instrumented mountainous site. *Ann. Glaciol.*, 51(54), 207–217.
9 doi:10.3189/172756410791386661.

10 Ôura, H., Ishida, T., Kobayashi, D., Kobayashi, S., and Yamada, T., 1967. Studies on blowing
11 snow: Part II. *Physics of Snow and Ice: Int. Conf. on Low Temperature Science*, Sapporo, Japan,
12 Institute of Low Temperature Science, Hokkaido University, 1099–1117.

13 Parish, T. R., and Bromwich D. H., 1987. The surface wind field over the Antarctic ice sheet.
14 *Nature*, 328, 51-54.

15 Parish, T. R., and Bromwich, D. H., 2007. Reexamination of the near-surface airflow over the
16 Antarctic continent and implications on atmospheric circulations at high southern latitudes.
17 *Monthly Weather Review*, 135, 1961-1973.

18 Parish, T. R., Pettré, P., and Wendler, G., 1993. The influence of large scale forcing on the
19 katabatic wind regime of Adélie Land, Antarctica. *Meteor. Atmos. Phys.*, 51, 165-176.

20 Pomeroy, J. W., Gray, D. M., and Landine, P. G., 1993. The prairie blowing snow model:
21 Characteristics, validation, operation. *J. Hydrol.*, 144, 165–192.

22 Raupach, M. R., 1992. Drag and drag partition on rough surfaces. *Boundary-Layer Meteorol.*,
23 60, 375-395.

24 Sato, T., Kimura, T., Ishimaru, T., and Maruyama, T., 1993. Field test of a new snow-particle
25 counter (SPC) system. *Ann. Glaciol.*, 18, 149–154.

26 Schmidt, R. A., 1980. Threshold wind-speeds and elastic impact in snow transport. *J. Glaciol.*,
27 26-94, 453–467.

1 Shao, Y., 2008. Physics and modelling of wind erosion. Springer Verlag.

2 Smith, J. D., and McLean, S. R., 1977. Spatially averaged flow over a wavy surface. *J. Geophys. Res.*, 82, 1735-1746.

4 Trouvilliez, A., Naaim-Bouvet, F., Genthon, C., Piard, L., Favier, V., Bellot, H., Agosta, C.,

5 Trouvilliez, A., Naaim-Bouvet, F., Bellot, H., Genthon, C., and Gallée, H., 2015. Evaluation of

6 FlowCapt acoustic sensor for snowdrift measurements. *J. Atmos. Ocean. Technol.*, 32(9), 1630-

7 1641.

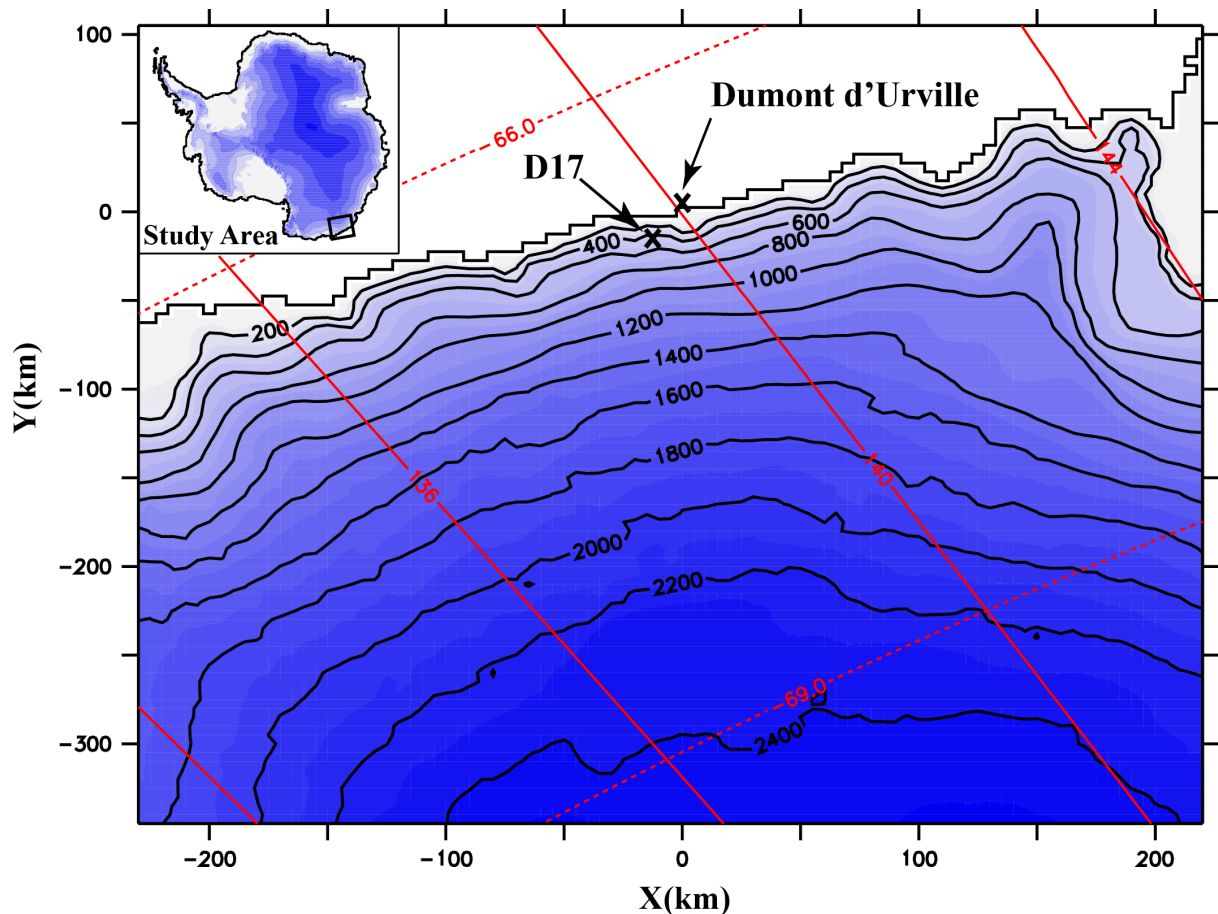
8 Wiberg, P. L., and Nelson, J. M., 1992. Unidirectional flow over asymmetric and symmetric

9 ripples, *J. Geophys. Res.*, 97(C8), 12745-12761.

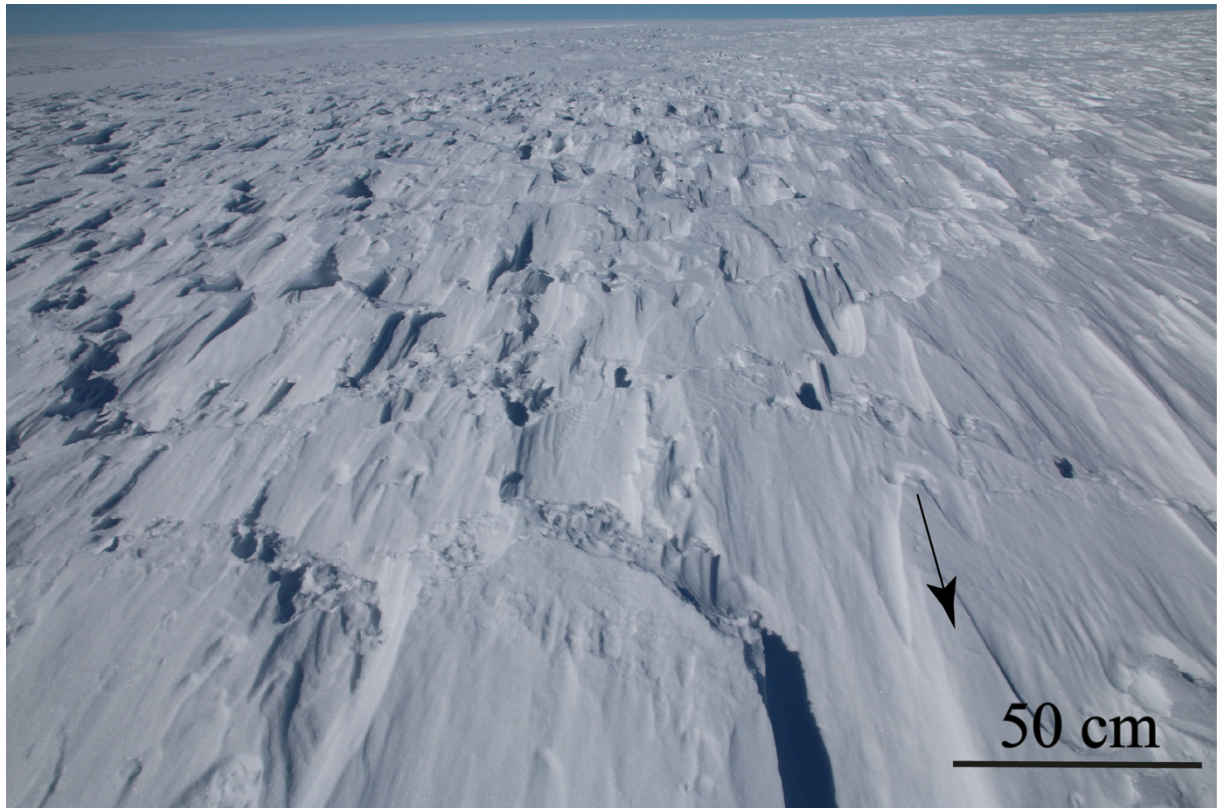
10 Wilkinson, R. H., 1984. A method for evaluating statistical errors associated with logarithmic

11 velocity profiles. *Geo-Mar. Lett.*, 3, 49–52.

12



1
2 **Fig. 1.** Map of Adélie Land showing the location of Dumont d'Urville station and measurement
3 site D17. Contour lines are in meters.



1

2 **Fig. 2.** Photograph of the snow surface at D17 in January 2014. The arrow indicates the mean
3 direction of the wind episode that led to the formation of the sastrugi.

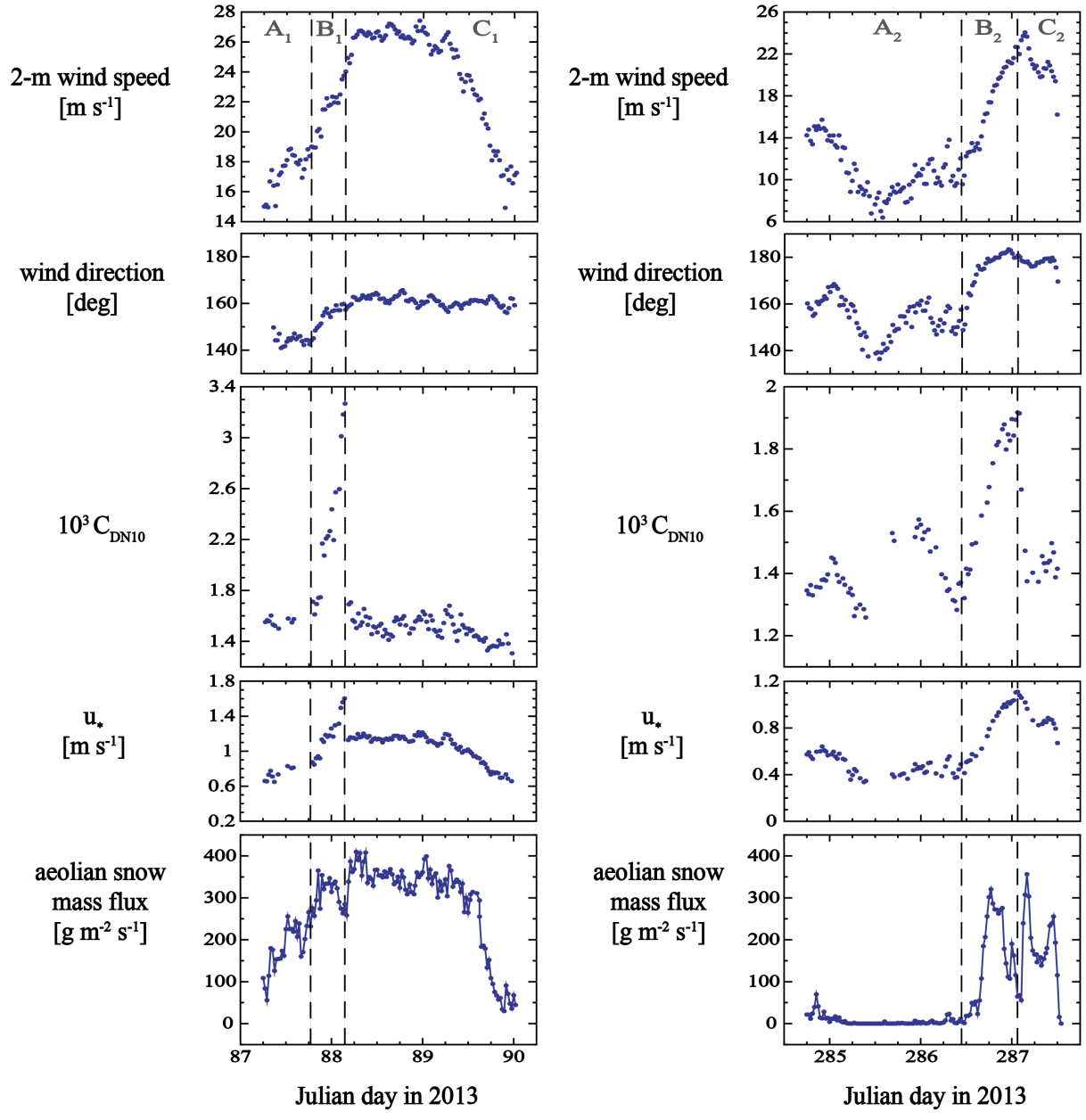


Fig. 3. Two erosion events showing sastrugi responses to shifts in wind direction. Note the different vertical scales between right and left panels concerning measured 2-m wind speed and profile-derived C_{DN10} and u_* values. The aeolian snow mass fluxes come from the second-generation FlowCaptTM sensor set up from 0 to 1 m above the snow surface. In both cases, the event is split into three parts, respectively before (A_i), during (B_i) and after (C_i) the wind shift.